Journal of Geophysical Research: Atmospheres

RESEARCH ARTICLE
10.1029/2018JD028585

Key Points:
- This paper quantifies and corrects two intersatellite calibration errors due to spectral gapping and finite spectral resolution
- These errors are scene dependent and could be significant
- The effectiveness of the correction method has been validated using both simulated and satellite-observed data

Correspondence to:
X. Liu,
xu.liu-1@nasa.gov

Citation:
Wu, W., Liu, X., Xiong, X., Li, Y., Yang, Q., Wu, A., et al. (2018). An accurate method for correcting spectral convolution errors in intercalibration of broadband and hyperspectral sensors. *Journal of Geophysical Research: Atmospheres*, *123*, 9238–9255. https://doi.org/10.1029/2018JD028585

Received 27 FEB 2018
Accepted 9 AUG 2018
Accepted article online 27 AUG 2018
Published online 9 SEP 2018

An Accurate Method for Correcting Spectral Convolution Errors in Intercalibration of Broadband and Hyperspectral Sensors

Wan Wu[1], Xu Liu[2], Xiaoxiong Xiong[3], Yonghong Li[4], Qiguang Yang[1], Aisheng Wu[4], Susan Kizer[1], and Changyong Cao[5]

[1]Science Systems and Applications, Inc., Hampton, VA, USA, [2]NASA Langley Research Center, Hampton, VA, USA, [3]Earth Sciences Directorate, NASA Goddard Space Flight Center, Greenbelt, MD, USA, [4]Science Systems and Applications, Inc., Lanham, MD, USA, [5]NOAA, Center for Satellite Application and Research, College Park, MD, USA

Abstract The intercalibration between a broadband and a hyperspectral satellite Earth observation system requires the convolution of the hyperspectral data with the spectral response functions (SRFs) of the corresponding broadband channels. There are two potential issues associated with the convolution procedure. First, the finite resolution of a hyperspectral spectrum, that is, the deviation from the highly accurate *line-by-line* monochromatic radiances, will contribute to convolution errors. The magnitude of the errors depends on the spectral resolution and the SRF shape of the hyperspectral instrument. This type of the convolution error has not been well recognized, and there is a lack of corresponding discussion in most published papers. Although it is small as compared with the instrument accuracy of existing hyperspectral sounders, the error is deemed to be significant when it is compared with the stringent calibration requirement imposed by future climate missions like the Climate Absolute Radiance and Refractivity Observatory. Second, some broadband channels are insufficiently covered by the hyperspectral data, causing spectral gaps that lead to convolution errors. Although several methods have been developed to fill the spectral gaps and hence compensate for the second type of convolution error, the correction accuracy may still need improvement especially when a large spectral gap needs to be filled. This paper presents a methodology to accurately quantify and compensate for both types of convolution errors. This methodology utilizes the available hyperspectral information to correct the scene-dependent convolution errors due to either the limited spectral resolution or spectral gaps. We use simulations to characterize the intercalibration errors between the Moderate resolution Imaging Spectroradiometer (MODIS) and current operational infrared sounders. We demonstrate that convolution errors can be effectively removed to meet the highly accurate intersatellite calibration requirement proposed by the Climate Absolute Radiance and Refractivity Observatory. Our methodology is also validated using real satellite data for the intercalibration between Aqua MODIS and Aqua Atmospheric Infrared Sounders (AIRS). Our study demonstrates that the accurate characterization and correction for the convolution errors greatly reduces the scene-dependent and spectrally dependent errors, being critical to the consistency check between Infrared Atmospheric Sounding Interferometer (IASI) and AIRS using the double-difference method. The convolution correction also facilitates the evaluation for other intercalibration errors (e.g., the drift of MODIS SRFs). Our derived SRF shift values from MODIS-AIRS (after convolution error corrections) and from MODIS-IASI intercalibration are consistent with each other. We further extend the methodology to study the calibration of a broadband channel which is either completely or largely uncovered by a hyperspectral measurement. The large spectral gap filling methodology is validated by demonstrating the accurate prediction of the MODIS radiance of band 29 using the Cross-track Infrared Sounder spectra, with the real IASI spectral data being used as the reference.

1. Introduction

Intercalibration of different satellite sensors using a high accuracy hyperspectral data is critical to ensure the accuracy and reliability in using satellite observations for weather, climate, and environmental applications. Hyperspectral sensors have much smaller spectral response uncertainties than broadband sensors. Using hyperspectral sounders to calibrate broadband infrared (IR) systems is an important part of the international intercalibration efforts that include the intercalibration between the geostationary satellites and low Earth-orbiting and the intercalibration between low Earth-orbiting sensors. In order to maximize the advantage provided by the hyperspectral instruments, intercalibration errors in principle should be minimized to be,

ideally, smaller than the radiometric calibration accuracy of the hyperspectral sensors. There are currently several hyperspectral IR sounders in orbit: the Infrared Atmospheric Sounding Interferometer (IASI-A and IASI-B) in a Sun-synchronous midmorning orbit, Atmospheric Infrared Sounders (AIRS), and Cross-track Infrared Sounder (CrIS) in an afternoon orbit. The IASI-A, IASI-B, and AIRS have been used as the hyperspectral intercalibration references in the Global Space-based Inter-Calibration System (Chander et al., 2013; Goldberg et al., 2011; Hewison et al., 2013). CrIS has also been accepted as one of the Global Space-based Inter-Calibration System references recently. Most recently, Hyperspectral Infrared Atmospheric Sounder that is carried by the FY-3D satellite has joined IASI and CrIS as the third Fourier transform spectrometer that can provide global scale atmospheric sounding. A lot of studies have been carried out in the past to characterize and/or correct the intercalibration errors between those hyperspectral sensors and other broadband sensors (Cao et al., 2009; Gunshor et al., 2009; Tobin et al., 2006; Wang & Cao, 2008; L. Wang et al., 2007, 2009, 2010, 2012; X. Wu & Yu, 2013; Yu & Wu, 2013). Although methodologies used in those studies have provided means to characterize and/or reduce the intercalibration errors, those studies are not aiming at achieving an intercalibration with *climate* accuracy. In the future, hyperspectral sensors like the Climate Absolute Radiance and Refractivity Observatory (CLARREO) with radiometric traceability to the International System of Units will provide on-orbit calibration for the existing Earth observation missions so that the measurement accuracy suitable for climate studies can be achieved (Wielicki et al., 2013). The spectral calibration accuracy of CLARREO is designed to calibrate other Earth observation missions with the desired *climate observation accuracy* (Liu et al., 2017). The ultrahigh calibration accuracy of CLARREO will impose much more stringent intercalibration accuracy requirement that may not be satisfied by the existing intercalibration schemes.

Intercalibration between hyperspectral and broadband sensors requires the use of synchronized, collocated, and viewing-geometry matched measurements. Any mismatch in those observation factors will introduce errors. In addition to spatial-temporal matching errors and calibration errors of both broadband and hyperspectral instruments, there is another potential error due to finite instrument spectral resolution and spectral gaps in the hyperspectral instrument. We call this error source as *spectral convolution error*. The intercalibration requires the transformation of hyperspectral measurements to *hyperspectral convolved* measurements with the same spectral response feature of the target broadband sensor. The transformation is typically done by convolving the spectral response function (SRFs) of the broadband sensor with the hyperspectral measurements. In the spectral domain,

$$R_v^k = \boldsymbol{R_h} \otimes \boldsymbol{S_b} = \int_{\upsilon_1^k}^{\upsilon_2^k} R_h(\upsilon) S_b(\upsilon) \mathrm{d}\upsilon \Big/ \int_{\upsilon_1^k}^{\upsilon_2^k} S_b(\upsilon) \mathrm{d}\upsilon, \tag{1}$$

where R_v^k represents the hyperspectral convolved broadband radiance measured by the kth broadband channel centered at wavenumber υ_k; $R_h(\upsilon)$ represents the hyperspectral channel radiance at wavenumber υ; and $\boldsymbol{S_b}$ is the SRF of the kth broadband channel with the band edges being defined by υ_1^k, υ_2^k. However, the radiance measured by the kth broadband channel is

$$R_b^k = \boldsymbol{R_m} \otimes \boldsymbol{S_b} = \int_{\upsilon_1^k}^{\upsilon_2^k} R_m\left(\upsilon'\right) S_b\left(\upsilon'\right) \mathrm{d}\upsilon \Big/ \int_{\upsilon_1^k}^{\upsilon_2^k} S_b\left(\upsilon'\right) \mathrm{d}\upsilon', \tag{2}$$

where $\boldsymbol{R_m}$ is the monochromatic radiance. The difference between the hyperspectral convolved broadband radiance, R_v^k, and the observed broadband radiance, R_b^k, is known as the convolution error. The convolution errors can be a limiting factor for the intercalibration accuracy and is the focus of this paper.

The causes of the convolution error, $\Delta R^k = R_b^k - R_v^k$, can be understood from two perspectives: the fundamental error is due to the difference between the hyperspectral channel radiance, $\boldsymbol{R_h}$, which has a finite spectral resolution, and the *line-by-line* monochromatic radiance, $\boldsymbol{R_m}$; the missing information due to the existence of spectral gaps introduces errors in R_v^k, also contributing to the overall convolution errors.

The convolution error caused by spectral gaps in hyperspectral measurements has been widely recognized and studied. The spectral gaps are spectral regions within a broadband channel that are not covered by the hyperspectral measurement. For example, Figure 1 demonstrates the spectral gaps in AIRS observations that will affect the Moderate resolution Imaging Spectroradiometer (MODIS)-AIRS intercalibration. AIRS is a hyperspectral grating spectrometer with 2,378 spectral channels covering the 650–1,136, 1,217–1,614, and

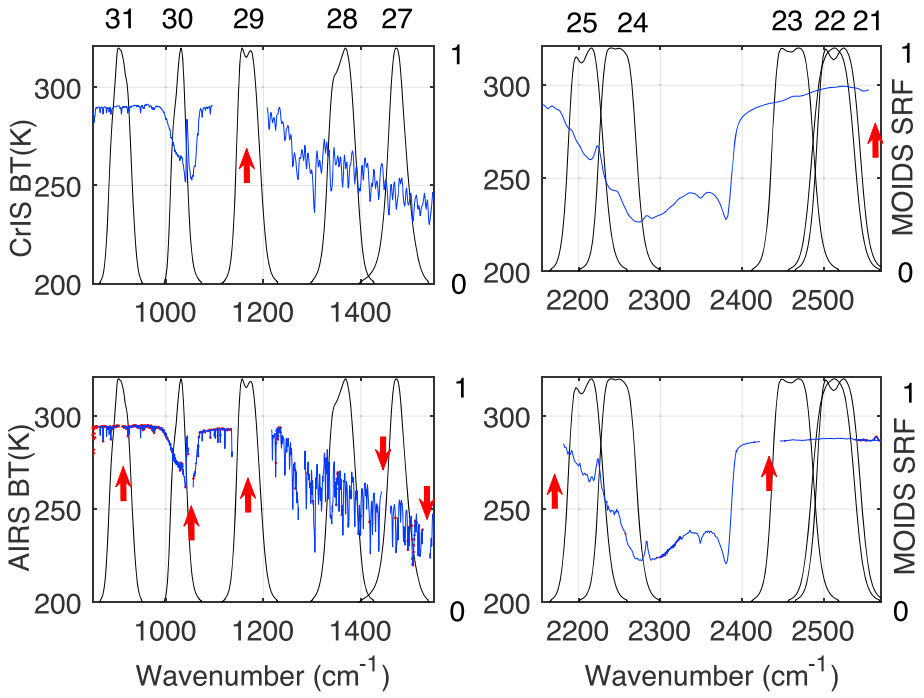

Figure 1. Spectral gaps of CrIS and AIRS in the MODIS infrared measurement band. The blue curves are typical CrIS and AIRS spectra in brightness temperature. The SRFs of MODIS are plotted as black curves with the spectral gaps (with a larger than 5 cm^{-1} frequency interval) marked using red arrows. MODIS band numbers are listed correspondingly. The red dots in the bottom row illustrate noisy AIRS channels where the measurement may fail the quality control and therefore cannot be used. CrIS = Cross-track Infrared Sounder; AIRS = Atmospheric Infrared Sounders; MODIS = Moderate resolution Imaging Spectroradiometer; SRFs = spectral response functions; BT = brightness temperature.

2,181–2,665 cm^{-1} spectral regions (Aumann et al., 2003). MODIS is a high–spatial resolution, multispectral scanning radiometer with 36 spectral bands. Sixteen of the MODIS bands have their central wavelengths in the IR spectral region (695–2,732 cm^{-1} Barnes et al., 1998). The hyperspectral channels of AIRS are not evenly distributed within the measurement bands. The spectral gaps illustrated in Figure 1 cover all regions where the interval between two adjacent hyperspectral channels is greater than 5 cm^{-1}. Figure 1 also demonstrates the spectral gaps of CrIS, a Fourier transform spectrometer that provides atmospheric sounding with 1,305 spectral channels, over three wavelength regions: 650–1,095, 1,210–1,750, and 2,155–2,550 cm^{-1} (Han et al., 2013; Lee et al., 2010).

To address the convolution errors introduced by spectral gaps, one can either fill the missing spectral region before the convolution transformation or apply corrections on the convolved radiances. Tobin et al. (2006) simulated the clear-sky radiances measured by AIRS and MODIS using six standard atmospheres as inputs. They calculated the convolution errors based on those simulation results, and the simulated bias values were used to correct the intercalibration of real measurements. This method successfully reduced some systematic errors but did not fully account for the scene-dependent uncertainties due to inadequate representation of the real atmospheric variations using the six standard atmospheres. Gunshor et al. (2009) used the U.S. Standard Atmosphere to simulate the missing spectra of AIRS and tried to compensate for the scene-dependent uncertainties according to the end points values of the spectral gaps; however, they pointed out that their method may not accurately address the variations of real atmosphere from the U.S. Standard Atmosphere, did not include cloudy spectra, and could fail when the end points of a spectral gap fall on an atmospheric absorption line. Tahara and Kato, (2008) derived a linear regression relationship between the observed channel radiances of the IASI or AIRS and the simulated radiances for eight atmospheric model profiles. Those eight atmospheric profiles included representative atmospheric profiles in various altitude regions under both clear and cloudy sky conditions. Their method improved the spectral gap filling accuracy by effectively addressing the scene-dependent feature of the convolution errors. It can fill in missing IASI and AIRS radiance channels for narrow spectral gaps. However, the usage of only eight sample spectra do not

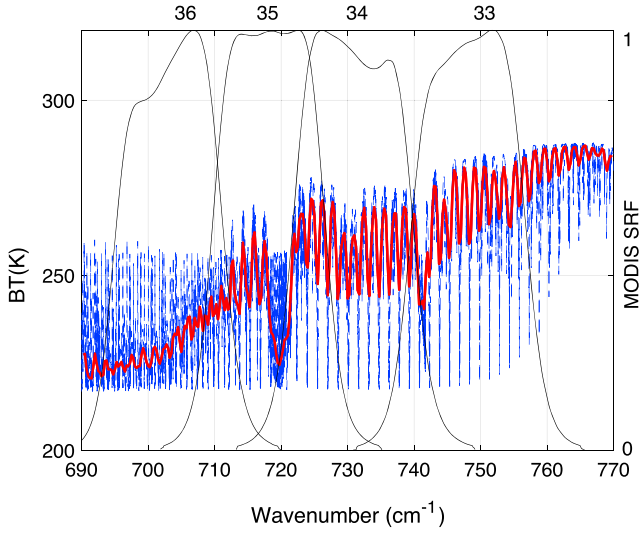

Figure 2. Sample Infrared Atmospheric Sounding Interferoeter spectrum in the CO_2 absorption region (red curve) in comparison with the line-by-line monochromatic spectrum (blue curve with a spectral sampling resolution of 0.0025 cm^{-1}). The Moderate resolution Imaging Spectroradiometer SRFs are plotted as references. SRFs = spectral response functions; BT = brightness temperature.

provide adequate account for the large scene variability and the gap-filling error gets large when the spectral gap becomes large.

In comparison to errors due to the spectral gaps, the convolution error caused by the finite spectral resolution of the hyperspectral measurements is less recognized. Theoretically, the radiance measured by a hyperspectral channel is

$$R_h(\upsilon_l) = \boldsymbol{R_m} \otimes \boldsymbol{S_h} = \int_{\upsilon_1^l}^{\upsilon_2^l} R_m\left(\upsilon'\right) S_h\left(\upsilon'\right) \mathrm{d}\upsilon \Big/ \int_{\upsilon_1^l}^{\upsilon_2^l} S_h\left(\upsilon'\right) \mathrm{d}\upsilon' \tag{3}$$

where $\boldsymbol{S_h}$ is the SRF of the lth hyperspectral channel that centers at wavenumber υ_l and spans from υ_1^l to υ_2^l. Using equations (1)–(3), the convolution errors can be calculated as

$$\begin{aligned} \Delta R^k &= (R_m \otimes S_h) S_b - R_m \otimes S_b \\ &= \left(\int_{\upsilon_1^k}^{\upsilon_2^k} R_h(\upsilon) S_b(\upsilon) \mathrm{d}\upsilon - \int_{\upsilon_1^k}^{\upsilon_2^k} R_m(\upsilon) S_b(\upsilon) \mathrm{d}\upsilon \right) \Big/ \int_{\upsilon_1^k}^{\upsilon_2^k} S_b(\upsilon) \mathrm{d}\upsilon \end{aligned} \tag{4}$$

If the spectral resolution of a hyperspectral measurement is high compared to the Doppler and Lorentz half widths, then the hyperspectral channel radiance becomes equivalent to the monochromatic radiance so that there is no convolution error due to the finite spectral resolution. In reality, the fundamental difference between R_h and R_m can be understood from two perspectives:

1. The finite resolution of hyperspectral measurements means that they cannot provide the equivalent spectral information as that embedded in the monochromatic spectra (as can be seen from Figure 2). Generally, a higher spectral resolution means a better approximation for the monochromatic radiance.
2. The magnitude of convolution errors also depends on the shape of the SRFs of hyperspectral sensors. There are spectral overlappings between channels of hyperspectral measurements. Figure 3 shows sample SRFs of the Blackman apodized CrIS measurement. Figure 4 demonstrates sample SRFs of the unapodized CrIS measurement. Strong local correlations exist in apodized measurements. Significant side lobes of an unapodized SRF can extend to nonnearby channels. Both situations complicate the relationship between the hyperspectral channel radiances and the monochromatic radiances defined in equation (3) and therefore contribute to the convolution errors expressed in equation (4).

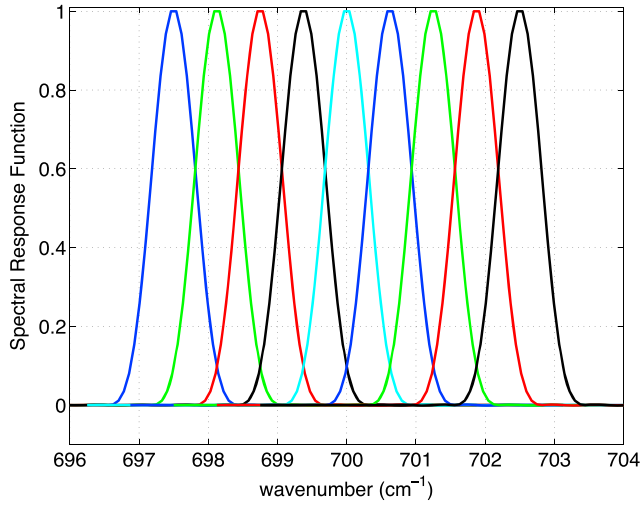

Figure 3. Sample spectral response functions of Cross-track Infrared Sounder measurement with Blackman apodization around 700 cm^{-1}.

There has been a lack of systematic characterization and corresponding correction for such convolution errors in the intercalibration studies. However, we demonstrate in section 3 that such errors need to be corrected for a high-accuracy intercalibration, like that proposed for the CLARREO mission. CLARREO is designed to serve as a high-accuracy, International System of Units-traceable calibration reference on orbit for other EO systems. CLARREO's radiometric calibration accuracy for the IR instrument will be in the range of 0.04–0.06 K (95% confidence interval) (Liu et al., 2017; Wielicki et al., 2013). This requirement is based on the climate trend detection uncertainty analysis. Due to the natural variabilities of climate variables such as atmospheric temperature and water vapor, it will take a certain length of time to detect an accurate trend even if there is no error in the observation system. The CLARREO instrument is designed so that the instrument calibration error will only add a minimum delay in the trend detection relative to a perfect observation system (Liu et al., 2017).

A correction algorithm that can be used to correct scene-dependent convolution errors is introduced in this paper. The algorithm uses a pretrained regression relationship and the available hyperspectral

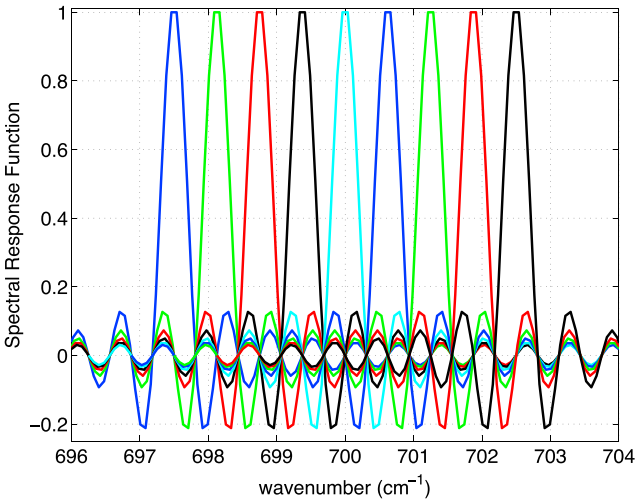

Figure 4. Sample spectral response functions of unapodized Cross-track Infrared Sounder measurement around 700 cm^{-1}.

information to predict the convolution errors or the missing spectral information. Section 3 shows that convolution errors can be estimated and corrected with a very high accuracy using this algorithm. The convolution errors for the intercalibration between MODIS and three operational sounders, that is, IASI, AIRS, and CrIS, are characterized using simulated results. We demonstrate that a high-accuracy correction for convolution errors due to either the small spectral gaps or the finite spectral resolution of the hyperspectral measurements can be achieved using the correction algorithm. To highlight the accuracy of our algorithm for the convolution error correction, we compare the residual errors after the correction with the calibration requirement defined by the CLARREO mission (Liu et al., 2017). We evaluate our algorithm by checking if the convolution errors larger than the CLARREO calibration requirement can be effectively corrected. We also illustrate the successful correction for convolution errors in the MODIS-AIRS intercalibration using the real data. We show in section 4 that the MODIS-AIRS (both on Aqua) intercalibration errors after the correction for convolution errors become consistent with the corresponding MODIS (Aqua)-IASI (Metop-A) intercalibration errors. The accurate characterization and correction for convolution errors avoid the overestimation or underestimation for the real instrument calibration errors and facilitate the investigation about potential contributors to MODIS calibration bias (e.g., potential spectral shifts in MODIS SRFs).

When a large portion of a hyperspectrum needed for the intercalibration of a broadband channel are missing, for example, the intercalibration between MODIS band 29 radiances and AIRS (or CrIS) spectra, the hyperspectral convolved broadband radiance, R_v^k, cannot be given directly. Therefore, large spectral gaps need to be filled for the intercalibration of corresponding broadband channels. Similar to the method used to estimate and correct the convolution errors, the regression relationship between existing spectra and spectral gaps is used to predict the latter. The accuracy of filling spectral gaps has a direct impact on the accuracy of the intercalibration. To evaluate the spectral filling accuracy, we validate the prediction for the IASI spectra in the 1,115–1,207 cm^{-1} region within the MODIS band 29 using the CrIS measurements that do not provide the spectral coverage.

Section 2 presents details about the regression-correction methodology. Section 3 systematically characterizes the convolution errors between MODIS and the hyperspectral IR sounders and demonstrates the correction for those large errors according to the CLARREO standard. Section 4 presents the application of the algorithm for the intercalibration between real satellite measurements of AIRS and MODIS. The spectral gap filling study for the intercalibration of MODIS band 29 using CrIS spectra is discussed in section 5.

2. Methodology

As is shown by equations (2)–(4) in section 1, the convolution errors can be viewed as a function of the true monochromatic radiance, $\boldsymbol{R_m}$, and the hyperspectral radiance, $\boldsymbol{R_h}$. There is a strong correlation relationship between the monochromatic radiance and the hyperspectral radiance. Therefore, a linear regression relationship between the convolution errors and the hyperspectral channel radiance can be derived. The regression relationship is established by using simulated broadband and hyperspectral radiances. Monochromatic spectra, $\boldsymbol{R_m}$, are calculated using the line-by-line code LBLRTM (Clough & Iacono, 1995). A total of 14,600 spectra are simulated using realistic geophysical properties under both clear sky and cloudy sky conditions. Half of the total spectra are daytime spectra which include the contribution from solar scattering, and the remaining half are nighttime spectra. The global distributed atmospheric temperature, water vapor, and other trace gas profiles with wide dynamic range are selected from databases that cover some extreme conditions. Both ice and water clouds are included in the simulation. The simulation for multiple scattering properties of ice and water clouds is done off-line using 32-stream DISORT (Stamnes et al., 1988) and incorporated into the forward radiative transfer calculation via an effective

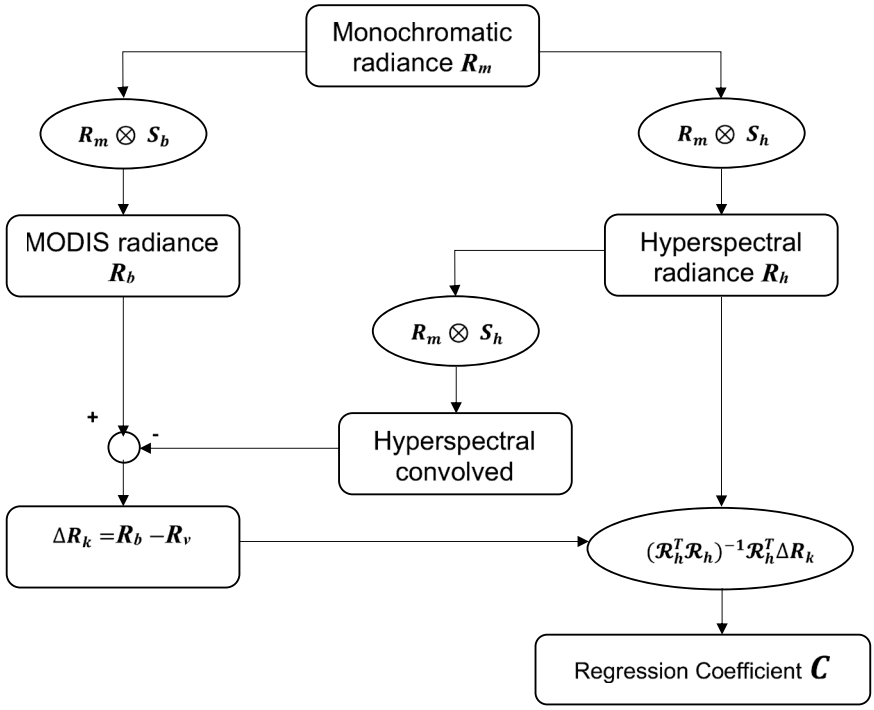

Figure 5. Flow diagram of the convolution error simulation process. MODIS = Moderate resolution Imaging Spectroradiometer.

parameterization scheme (Liu et al., 2009; W. Wu et al., 2017). The cloud top heights are randomly distributed in a range from close to surface to 50 hPa. The spectra include simulated observations of both over land and over water. The simulation covers the observations under various viewing geometry conditions, with satellite zenith angle ranges from −60° to 60°.

Following equations (2)–(4), we calculate the MODIS band radiances, $\boldsymbol{R_b}$, the convolution errors, $\Delta \boldsymbol{R^k}$, and the hyperspectral radiances, $\boldsymbol{R_h}$, for IASI, AIRS, and CrIS, respectively. Figure 5 shows the flow diagram of the convolution error simulation process. The regression relationship between the convolution errors of the *k*th broadband and the corresponding hyperspectral radiances (within the *k*th MODIS band) is mathematically defined as

$$\Delta \boldsymbol{R^k} = \boldsymbol{C R_h} = \sum_{i=1}^{nch} \boldsymbol{C_i}\, \boldsymbol{R_h}(\boldsymbol{i}), \tag{5}$$

where ***nch*** is the number of hyperspectral channel radiances within the *k*th MODIS band. The regression coefficient vector *C* is obtained using a linear least squares regression method,

$$C = \left(\mathcal{R}_h^T \mathcal{R}_h\right)^{-1} \mathcal{R}_h^T \Delta \boldsymbol{R^k}, \tag{6}$$

where $\Delta \boldsymbol{R^k}$ represents the ensemble of convolution errors $[\Delta \boldsymbol{R^k}(\boldsymbol{1}), \ldots, \Delta \boldsymbol{R^k}(\boldsymbol{N})]$ and $\mathcal{R}_h$ represents the ensemble of hyperspectral radiances $[\boldsymbol{R_h^1}, \ldots, \boldsymbol{R_h^N}]$; *N* is the total number of training samples.

In addition to the direct correction for convolution errors, a similar method can be applied to fill large spectral gaps. The direct convolution correction application using equation (6) may not work when most or all of the hyperspectral radiances within a certain band are not covered by a measurement (e.g., the intercalibration between AIRS or CrIS and MODIS band 29). For those cases, the available spectral radiances outside of a large spectral gap can be used to predict the missing channel radiances in the spectral gap,

$$\boldsymbol{R_h^{gap}} = \boldsymbol{A R_h^{available}}, \tag{7}$$

and *A* can be determined by

Table 1
Summary of Convolution Errors for the Intercalibration Between MODIS and Hyperspectral Sensors (IASI, CrIS, and AIRS)

MODIS band	Convolution errors (mean ± std (mK))					
	IASI	CrIS (FSR) unapodized	CrIS (FSR) Blackman	CrIS (NSR) unapodized	CrIS (NSR) Blackman	AIRS[a]
21	0.06 ± 0.04	−24.27 ± 10.04	−50.21 ± 20.07	−22.23 ± 9.98	−45.62 ± 19.95	2.49 ± 1.96
22	0.05 ± 0.03	−58.75 ± 23.11	−120.33 ± 45.87	−58.06 ± 24.05	−116.52 ± 45.50	2.37 ± 3.54
23	−0.02 ± 0.01	0.00 ± 0.36	−0.12 ± 0.09	−0.032 ± 0.09	−1.64 ± 2.34	37.30 ± 33.58
24	−0.64 ± 0.38	−0.22 ± 0.28	−3.18 ± 0.21	9.47 ± 5.14	−40.45 ± 25.56	25.68 ± 16.53
25	−0.24 ± 0.18	−0.14 ± 0.10	−1.14 ± 0.89	7.27 ± 4.16	−10.75 ± 10.99	499.90 ± 283.98
27	0.20 ± 0.07	−0.30 ± 0.17	0.28 ± 0.28	0.24 ± 0.21	1.89 ± 1.46	−1141.21 ± 717.28
28	−0.13 ± 0.09	0.03 ± 0.07	−0.57 ± 0.43	−0.33 ± 0.37	−2.2 ± 1.5	−78.48 ± 53.83
30	−0.01 ± 0.07	1.43 ± 1.20	−1.40 ± 1.05	1.43 ± 1.20	−1.40 ± 1.05	−40.09 ± 37.06
31	−0.02 ± 0.05	−0.03 ± 0.02	−0.12 ± 0.08	−0.03 ± 0.02	−0.12 ± 0.08	−80.08 ± 112.59
32	0.20 ± 0.22	−0.21 ± 0.04	0.93 ± 1.40	−0.21 ± 0.40	0.93 ± 1.40	30.97 ± 43.97
33	−2.27 ± 1.88	0.33 ± 0.17	−13.44 ± 11.55	0.33 ± 0.17	−13.44 ± 11.55	−176.72 ± 120.82
34	3.82 ± 3.11	2.87 ± 2.08	23.65 ± 19.28	−2.87 ± 2.08	23.65 ± 19.28	−233.66 ± 150.21
35	1.62 ± 1.20	0.87 ± 0.51	16.05 ± 11.11	−0.87 ± 0.51	16.05 ± 11.11	31.09 ± 20.05
36	−1.23 ± 0.73	0.15 ± 1.99	−8.81 ± 5.48	0.15 ± 1.99	−8.81 ± 5.48	−0.04 ± 0.45

Note. MODIS = Moderate resolution Imaging Spectroradiometer; IASI = Infrared Atmospheric Sounding Interferometer; CrIS = Cross-track Infrared Sounder; AIRS = Atmospheric Infrared Sounders; std = standard deviation; FSR = full spectral resolution; NSR = nominal spectral resolution.
[a]MODIS-AIRS convolution errors are obtained with more than 400 AIRS noisy channels being excluded.

$$A = \mathscr{R}_h^{\text{gap}} \mathscr{R}_h^{\text{available}} \boldsymbol{T} \left(\mathscr{R}_h^{\text{available}} \mathscr{R}_h^{\text{available}} \boldsymbol{T} \right)^{-1}. \tag{8}$$

Here A is a nch2 by nch1 matrix. The number of available hyperspectral channels is nch1, and the number of channels in the spectral gap region is nch2. This method works when there are correlations between the available spectral radiances outside of the gap and the missing spectral gap radiances. As we are going to discuss in section 5, the hyperspectral radiances within the MODIS band 29 can be well predicted using the available CrIS spectral outside of the MODIS band 29. As compared with Tahara's method described in section 1, this method uses a large number of spectra samples to better account for the scene variability. The prediction for spectral gap radiances is channel dependent. Unlike Tahara's method where a different regression coefficient has to be obtained for each observation, the spectral correlation relationship is defined using a fixed regression coefficient matrix A, which was trained in an offline process. Therefore, the implementation of this method for the gap radiance prediction is faster and easier.

3. Characterization and Correction for Convolution Errors

After using LBLRTM to simulate 14,600 monochromatic spectra, the corresponding hyperspectral radiances and MODIS band measurements are obtained by convolving the monochromatic spectra with the hyperspectral and broadband SRFs, respectively. equation (4) is used to calculate the convolution errors discussed in section 2. Table 1 lists the mean and the standard deviation (std) values of the convolution errors based on these 14,600 simulated cases. These cases cover a wide range of globally distributed observation scenes. The mean value corresponds to the bias that would be introduced into the intercalibration of each MODIS band even after averaging over a large number of collocated events. The std defines the variation range of the convolution errors.

IASI has a 0.25 cm^{-1} spectral sampling interval with a 0.5 cm^{-1} apodized spectral resolution. The magnitude of the convolution errors for all MODIS bands is in the order of millikelvin (mK) or less. As compared with the CLARREO's spectral calibration requirement of 0.02–0.03 K (k = 1, 68.3% confidence level), the convolution errors for the intercalibration between MODIS and IASI are small enough and will not pose as significant calibration errors.

The convolution errors for the MODIS-CrIS intercalibration are much larger than that for MODIS-IASI, due to the lower spectral resolution and spectral gaps in CrIS measurement. The spectral resolution for three measurement bands of CrIS in nominal spectral resolution (NSR) mode are 0.625 for longwave IR (LWIR), for midwave IR 1.25 for shortwave IR (MWIR), and 2.5 cm^{-1} (SWIR), respectively. In December 2014, the

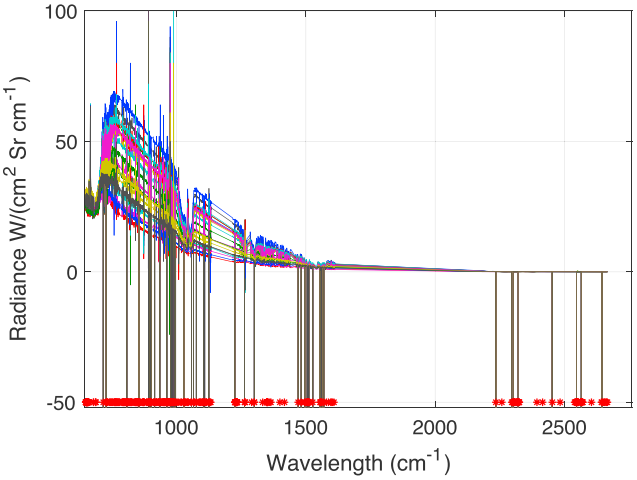

Figure 6. Sample Atmospheric Infrared Sounders spectra that include the radiance of bad channels (the bad channels are marked with red asterisks).

National Oceanic and Atmospheric Administration started to operate the Suomi National Polar-orbiting Partnership S-NPP CrIS in the full spectral resolution (FSR) mode (Chen & Han, 2015), in which the MWIR and SWIR bands have the same spectral resolution (0.625 cm^{-1}) as the LWIR band. MODIS bands 21–28 are calibrated using the MWIR and the SWIR measurement of CrIS, and bands 30–36 are calibrated using the LWIR measurement of CrIS. When a FSR CrIS spectrum is used to calibrate MODIS, the convolution errors of MODIS bands 23–28 become smaller due to the improved CrIS spectral resolution. When the same sampling resolution is used for all spectral bands, that is, the case for FSR CrIS, the convolution errors associated with the MODIS bands 33–36 (in the CO_2 absorption region) are larger than that for MODIS bands 23–32 (in atmospheric window spectral regions with relatively small spectral features). It reflects the fact that the variation in the monochromatic radiance in the CO_2 absorption region deviates more from that which can be captured by the hyperspectral measurement (see Figure 2). The same characteristics can be seen in MODIS-IASI convolution errors. Except for the convolution errors of bands 21 and 22, the errors for other bands are simply due to the limited spectral resolution and the spectral overlapping among adjacent channels of the CrIS measurement. The convolution errors for apodized CrIS measurement of bands 24, 25, 33, 34, 35, and 36 can still be viewed as significant as compared with the CLARREO calibration requirement (0.02–0.03 K). The corresponding errors for unapodized CrIS measurements are much smaller. This is because the spectral overlapping between adjacent SRFs of Blackman apodization (see Figure 3) is larger than that of the unapodized SRFs (see Figure 4). For both apodized and unapodized CrIS measurements, the band 21 and band 22 errors are in similar scale, indicating that

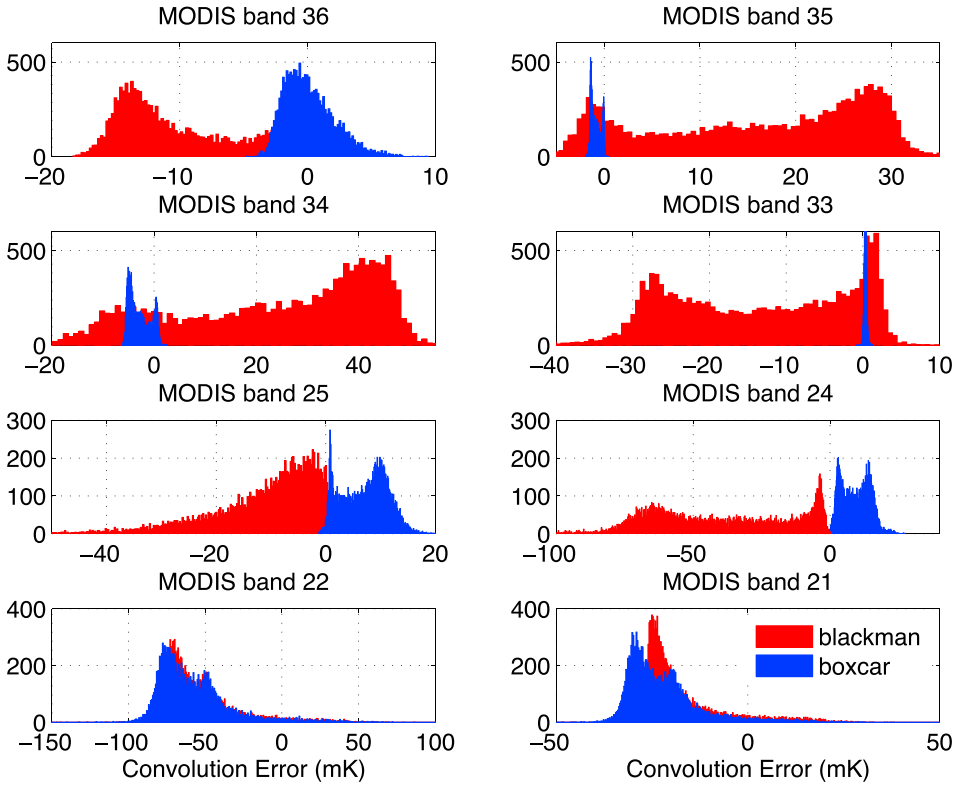

Figure 7. Distribution of convolution errors for the intercalibration between MODIS and nominal spectral resolution CrIS (simulation study results). Blue histogram = errors for unapodized CrIS meassurements red histogram = errors for CrIS measurements with Blackman apodization; MODIS = Moderate resolution Imaging Spectroradiometer; CrIS = Cross-track Infrared Sounder.

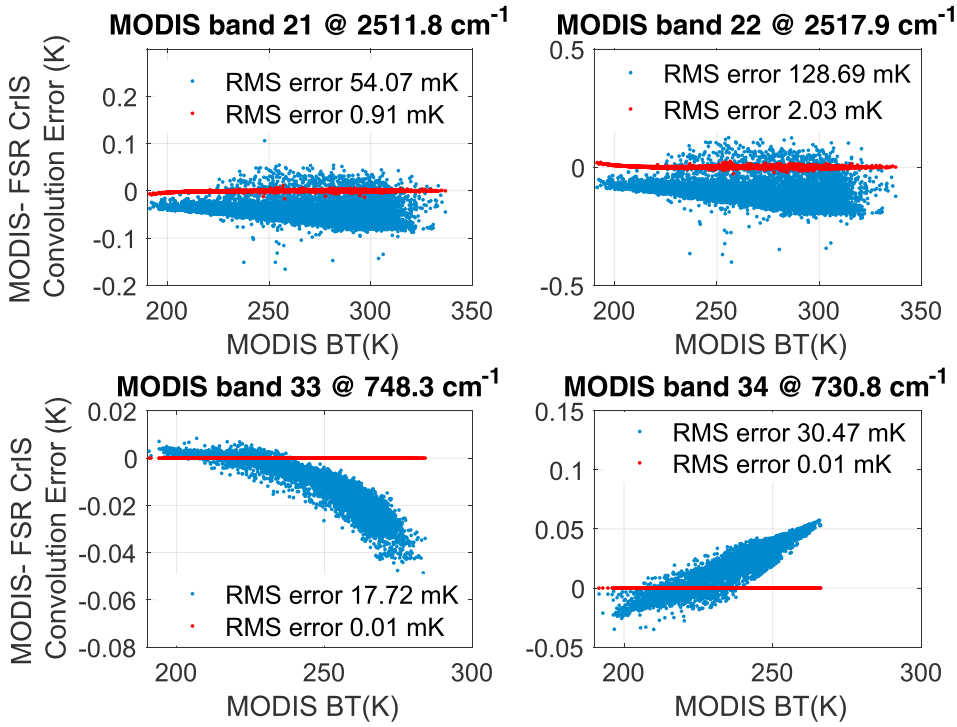

Figure 8. Convolution error correction for the intercalibration between the MODIS measurements of bands 21, 22, 33, and 34 and the FSR Blackman apodized CrIS measurements (simulation study results). Blue scatterplots = convolution errors before correction; red scatterplots = convolution errors after correction. The root-mean-square (RMS) values of the errors are listed accordingly. MODIS = Moderate resolution Imaging Spectroradiometer; CrIS = Cross-track Infrared Sounder; FSR = full spectral resolution; BT = brightness temperature.

the spectral gap (see Figure 1), rather than the apodization difference, is the dominant factor responsible for the convolution errors.

AIRS is a grating spectrometer with an unevenly distributed spectral grid spacing in wavenumber unit. Besides the MODIS band 29 which is largely uncovered by the AIRS measurement, MODIS bands 23, 25, 27, 30, and 31 are not sufficiently covered due to the spectral gaps with a spectral interval larger than 5 cm^{-1}. These gaps are due to nonoverlapping spectral converge between different detector arrays and due to the removal of channels with non-Gaussian noise (popping noise) in many of the AIRS detector array elements. Figure 6 shows sample radiance spectra from AIRS measurements on 17 September 2007. In order to strictly ensure the quality of the spectral information, measurements from more than 400 bad channels may not be used. Therefore, the AIRS spectral coverage for MODIS bands 28, 32, 33, 34, and 35 can also be distorted due to the missing information of bad channels. The convolution errors for the MODIS bands listed above are all significantly large according to the CLARREO standard.

Although the convolution errors are quantified by mean and std values listed in Table 1, it is noted that they are not randomly distributed errors. Figure 7 uses the intercalibration between MODIS bands 21, 22, 24, 25, 33, 34, 35, and 36 and CrIS (NSR) as examples to demonstrate the dependence of convolution errors on observation scenes. The distribution of convolution errors varies from instrument to instrument, and from band to band, being illustrated by the difference between Blackman apodized CrIS and the unapodized CrIS and the difference between different MODIS bands. The histograms demonstrate that convolution errors can be better characterized by a multimodal distribution than a random distribution. Such kind of errors cannot be effectively corrected using simple bias correction or large-sample averaging but can be well corrected using the algorithm described in section 2. Figure 8 demonstrates examples of using our method to correct the convolution errors for the intercalibration between MODIS bands 21, 22, 24, and 34 and the apodized CrIS in FSR mode. Figure 9 demonstrates the correction for the intercalibration between MODIS bands 28, 32, 33, 34, and 35 and AIRS. Our simulation study demonstrates that the convolution correction scheme

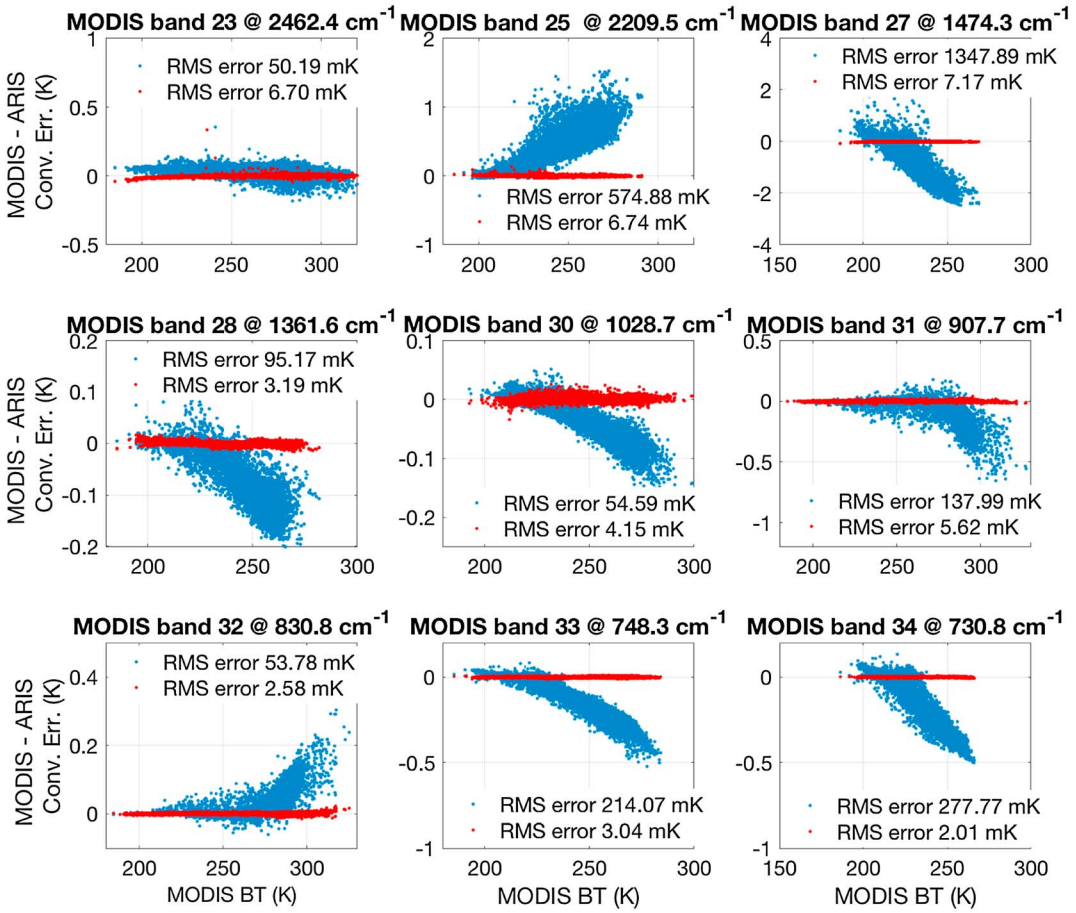

Figure 9. Convolution error correction for the intercalibration between the MODIS measurements of bands 23, 25, 27, 28, 30, 31, 32, 33, and 34 and the corresponding AIRS measurements (simulation study results). Blue scatterplots = convolution errors before correction; red scatterplots = convolution errors after correction. The root-mean-square (RMS) values of the errors are listed accordingly. The RMS errors listed in the subplots are in correspondence with the quadratic sum of the mean and standard deviation of the AIRS values stated in Table 1. MODIS = Moderate resolution Imaging Spectroradiometer; AIRS = Atmospheric Infrared Sounders; BT = brightness temperature.

effectively reduces the errors for all these cases to become orders of magnitude smaller than that required by the CLARREO mission.

4. Application on Real AIRS/MODIS Data

Collocated MODIS-AIRS and MODIS-IASI nadir data sets are used to test the convolution correction algorithm. Both MODIS and AIRS are carried by Aqua satellite, and their observations are always simultaneous. In principle, the results shown in this section for the MODIS-AIRS intercalibration should also work for the off-nadir observations since we trained our algorithm for ±60° viewing zenith angles. Considering that the MODIS-IASI convolution errors are negligible (see Table 1), the collocated MODIS-IASI intercalibration results can be used to validate the correction for the MODIS-AIRS convolution errors. The MODIS Level-1B Thermal Emissive Band product has 1 km resolution at nadir, while AIRS and IASI provide measurements with a spatial resolution of 13 and 12 km at nadir, respectively. The MODIS-AIRS data sets consist of AIRS spectra taken from six footprints located around the center of a scan (within a range of ±3.3° from nadir) and MODIS pixel radiances within a range of ±10.0° from nadir. For each AIRS footprint, MODIS pixels that lie within a 6.75 km radius around the center of the AIRS nadir footprint are selected. The aggregated value of those MODIS pixel radiances is used for the intercalibration. Typically, one AIRS footprint includes 140 MODIS pixels. We select AIRS footprints that are covered by more than 120 MODIS pixels to ensure the spatial coverage of the MODIS measurements for

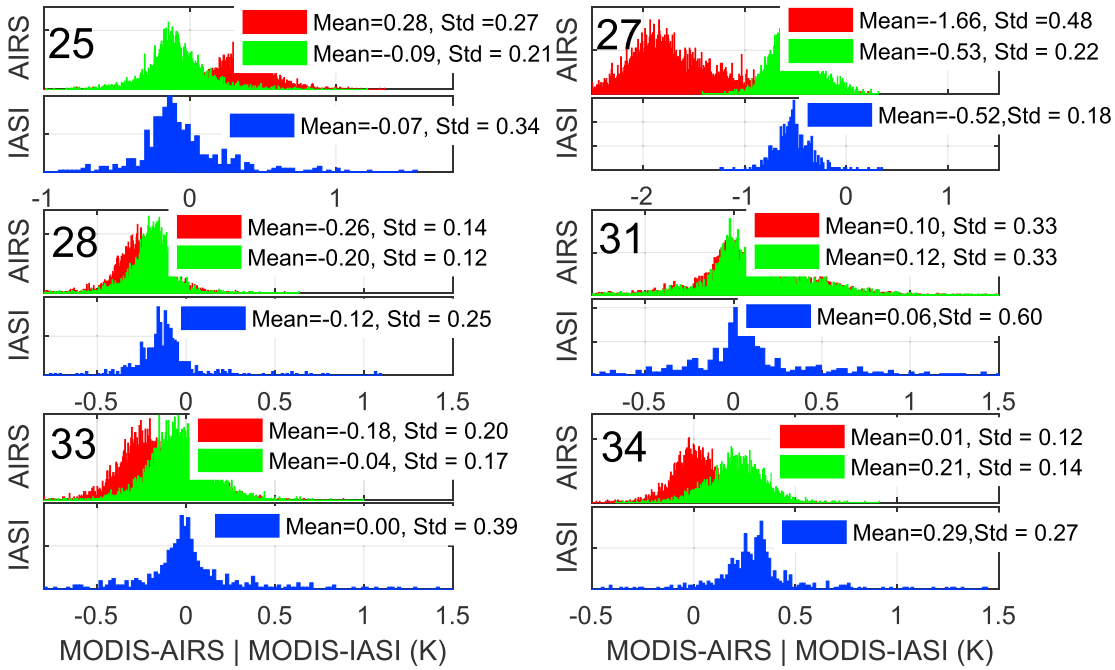

Figure 10. Comparison between the MODIS-AIRS intercalibration errors (of MODIS bands 25, 27, 28, 31, 33, and 34) after the convolution correction with the corresponding MODIS-IASI intercalibration errors from the Simultaneous Nadir Overpass observations on 1 July 2008. Red histograms = MODIS-AIRS intercalibration errors without correction for convolution errors; green histograms = MODIS-AIRS intercalibration errors after the convolution correction; blue histograms = MODIS-IASI intercalibration errors. Total number of collocated MODIS-AIRS samples is 3,690. Total number of collocated MODIS-IASI samples is 928. MODIS = Moderate resolution Imaging Spectroradiometer; AIRS = Atmospheric Infrared Sounders; IASI = Infrared Atmospheric Sounding Interferometer.

each AIRS footprint. When AIRS spectra are used to calculate the *convolved* MODIS band radiances, low quality AIRS channels are removed based on the channel quality assurance property given in AIRS Version 5 Documentation (2016). Specifically, only the channels with a quality assurance value less than 3 were used. Similar approaches have been used for various other studies and therefore been confirmed as an efficient and reliable method suitable for the MODIS-AIRS intercalibration study here (Efremova et al., 2014; Li et al., 2013; Li et al., 2016; A. Wu et al., 2012). The Simultaneous Nadir Overpass (SNO) data sets of IASI and MODIS are collected from two pairs of IASI footprints from each side of nadir and MODIS pixels in a range of ±10° near the nadir frame. The time difference for each MODIS-IASI SNO event is limited to be within 30 s. The radiances of all MODIS pixels located within a 6-km radius of an IASI footprint center are averaged to match the IASI observation. The Metop-A satellite's *morning* orbit only crosses with the Aqua orbit at approximately ±73.9° latitude line. There are limited number of MODIS-IASI SNO samples within 1 day. Instead of collecting SNO data with a rigorous temporal and spatial collocation relationship between IASI and AIRS, we collect the MODIS-AIRS samples within a ± 2.4° latitude zone near the ±73.9° latitude line for the study.

The hyperspectral measurement convolved MODIS radiances are calculated from IASI and AIRS observations following equation ((1)). The convolution of IASI and AIRS spectra with MODIS SRFs follows the trapezoidal integration rule (sample SRFs defined in wavenumbers are plotted in Figure 1). Those convolved radiances are then compared with the collocated MODIS radiances to obtain MODIS-IASI and MODIS-AIRS intercalibration errors. Considering that those are nadir observations, the convolved radiances are compared with the mean value of the radiances from the aggregated MODIS pixels that fall within the AIRS or IASI single field of view. The comparison between MODIS-IASI and MODIS-AIRS intercalibration of 1 July 2008 is demonstrated in Figure 10. We focus on the calibration for MODIS bands (25, 27, 28, 31, 33, and 34) which have the largest convolution errors according to our simulation study (see Table 1). Figure 10 confirms the accurate correction for the MODIS-AIRS convolution error that is demonstrated as the reduction in the systematic difference between the MODIS-IASI and MODIS-AIRS. A great measurement consistency between AIRS and IASI can be achieved after applying the convolution correction for the MODIS-AIRS intercalibration using the

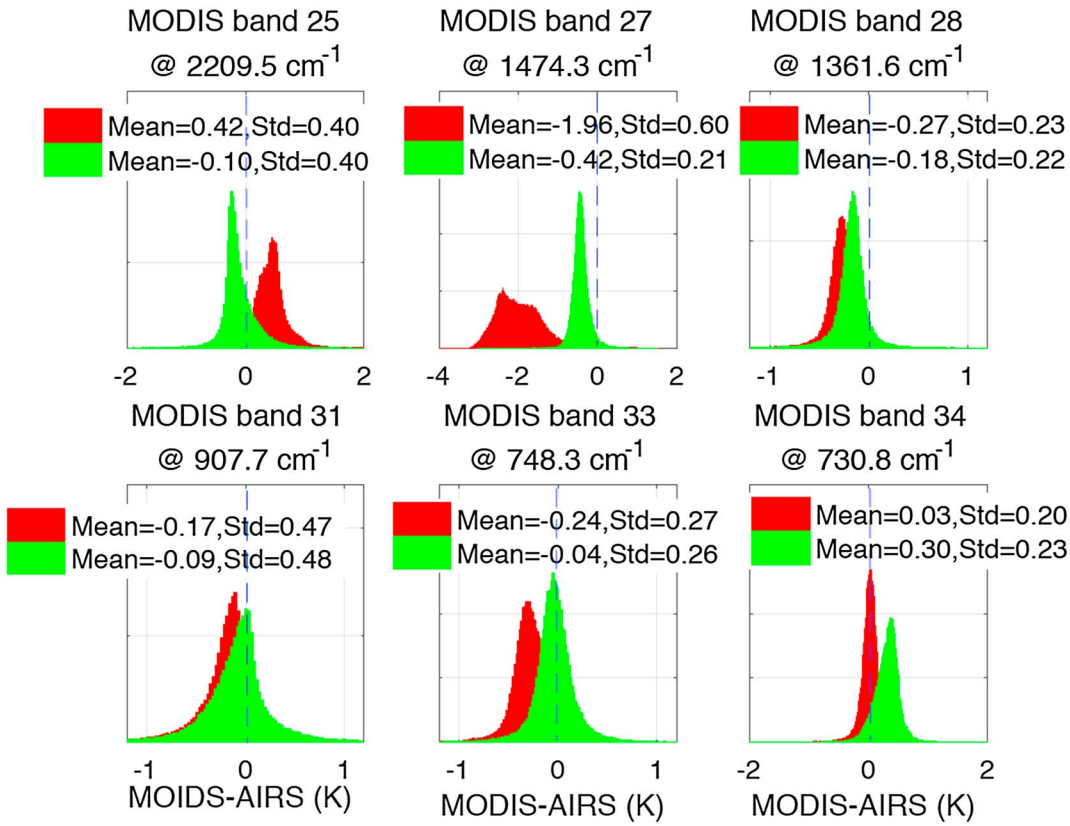

Figure 11. Intercalibration errors between MODIS measurements of bands 25, 27, 28, 31, 33, and 34 and the Simultaneous Nadir Overpass AIRS spectra measured on 17 September 2007. Red histograms = MODIS-AIRS intercalibration errors before the convolution correction; green histograms = MODIS-AIRS intercalibration errors after the convolution correction. MODIS = Moderate resolution Imaging Spectroradiometer; AIRS = Atmospheric Infrared Sounders.

regression coefficients from the simulation study. Before the convolution error correction, the systematic difference between IASI convolved radiance and AIRS convolved radiance is larger than 0.1 K for MODIS bands 25, 27, 28, 33, and 34 (see red and blue histograms in Figure 10). Band 27 has the largest MODIS-AIRS intercalibration error of 1.1 K, which is consistent with the simulation results. Despite the data sampling difference, the systematic difference between the IASI and the AIRS calibrated MODIS observations in those MODIS bands can all be reduced to be smaller than 0.1 K by applying the correction for the MODIS-AIRS convolution errors. The correction is more effective when the convolution error is the dominant error source of the MODIS-AIRS intercalibration errors (e.g., MODIS bands 25 and 27). It is interesting to see that the small intercalibration errors (0.01 K) between AIRS and MODIS band 34 is actually the combined effect of the convolution error and the real MODIS measurement error with a 0.21 K bias. This value is smaller than the collocated MODIS-IASI mean bias error of 0.29 K, indicating that IASI radiances are 0.08 K smaller than the collocated AIRS radiances near 730.8 cm^{-1} spectral region. This is consistent with the 0.088 K value derived from double-difference comparisons between GOES12 band 6 and AIRS and IASI radiances (L. Wang et al., 2010). This study provides a good example why an accurate convolution correction is needed in order to reveal some hidden intercalibration issues.

Since the Aqua and Metop-A satellites have limited SNO opportunities, we choose to further demonstrate our convolution error correction algorithm by using aggregated MODIS-AIRS global data taken from the Aqua satellite on 17 September 2007. Figure 11 illustrates the accurate convolution correction for the MODIS-AIRS intercalibration using these data. The multimodal distribution feature of the convolution errors for bands 25 and 27, which is scene dependent (see Figure 9), becomes very obvious in these global-distributed observations. The convolution correction clearly reduces the systematic biases for the calibration of five bands (25, 27, 28, 31, and 33). The distributions of intercalibration errors of bands 25, 27, 28, and 33 after the correction become more randomly distributed and less scene dependent, demonstrating the effective

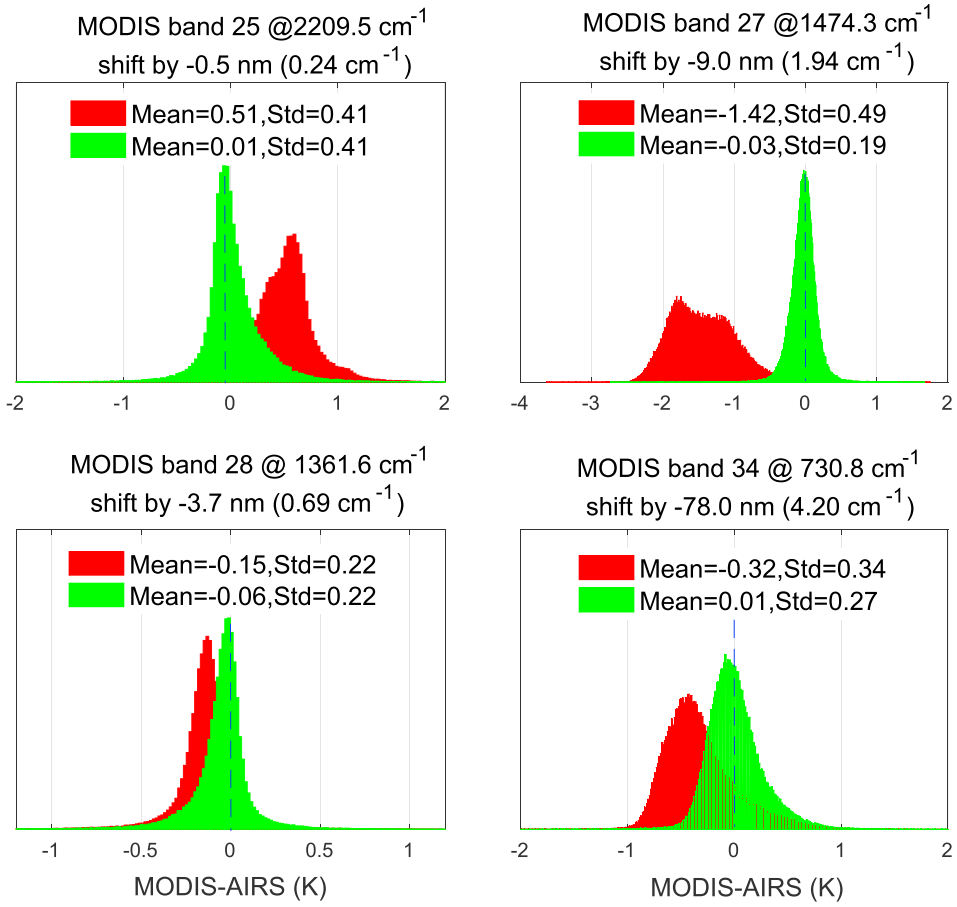

Figure 12. In correspondence to Figure 14 but for the convolution correction after shifting the spectral response functions of MODIS bands 25, 27, 28, and 34 by −0.5, −9.0, −3.7, and −78.0 nm, respectively. MODIS = Moderate resolution Imaging Spectroradiometer; AIRS = Atmospheric Infrared Sounders.

removal of convolution errors. It should be noted that even after the convolution error corrections, there are still residual errors such as random instrument noise, temporal-spatial matching error, and systematic calibration errors of the MODIS and the AIRS instrument themselves.

The spectral shift of MODIS SRFs has been suspected as a cause for the discrepancy between MODIS and IASI measurements (Sohn et al., 2010). The magnitude of the spectral shift for each MODIS band can be determined based on the MODIS-IASI intercalibration errors shown in Figure 10, that is, the SRF shifts are optimized to eliminate the bias of MODIS-IASI difference. For the MODIS-AIRS intercalibration, the same SRF shifts of MODIS are applied before the convolution correction. Figure 12 illustrates that the combined consideration for both the SRF shifts and the convolution errors can provide a very accurate compensation for the difference between AIRS and MODIS observations in both CO_2 and water vapor bands (MODIS bands 25, 27, 28, and 34). It is noted here that the −78.0 nm (~4.2 cm^{-1}) SRF shift demonstrated in the lower right subplot of Figure 12 seems to be large, although it effectively offsets the convolution errors between MODIS band 34 and AIRS. It is possible that there are other uncharacterized MODIS measurement error sources besides the SRF shifting. The validation for the spectral shift hypothesis requires additional information about other instrument related issues such as the radiometric nonlinearity (Xiong et al., 2009), electronic crosstalk (Sun et al., 2014), and out-of-band filter leaks (M. Wang et al., 2016).

Using only the SRF shifting to account for the scene-dependent intercalibration errors has been evaluated (Tobin et al., 2006). However, our study here reveals that the convolution error is a critical component of the scene-dependent intercalibration errors so that the SRF shifting effect can be overestimated without an accurate correction for convolution errors. By comparing Figure 12 with Figure 11, we can separate the convolution error from the error due to the potential SRF shifts. The top middle subplot in Figure 11 shows

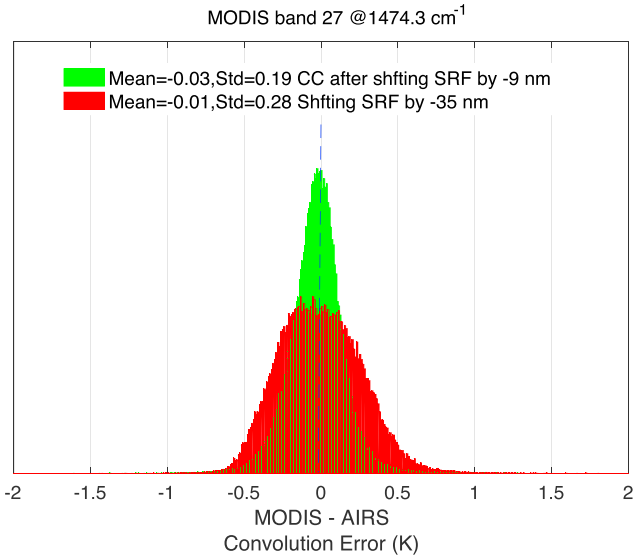

Figure 13. MODIS (band 27) minus AIRS brightness temperature difference after compensating for the intercalibration errors via two means: green histogram = applying convolution correction after shifting the MODIS SRF by −9.0 nm (~2.0 cm^{-1}); red histogram = shifting the MODIS SRF by −35.0 nm (~7.7 cm^{-1}); CC = convolution correction; MODIS = Moderate resolution Imaging Spectroradiometer; AIRS = Atmospheric Infrared Sounders; Std = standard deviation; SRFs = spectral response functions.

that the convolution correction without the SRF shifting of MODIS band 27 can already reduce the calibration bias by ~1.5 K (out of a total bias close to 2.0 K). Therefore, the convolution errors make up the major component of the total scene-dependent intercalibration errors in some cases. Figure 13 further compares the compensation for the MODIS-AIRS (band 27) difference via two means: (1) by applying convolution correction along with shifting the MODIS SRF by −9.0 nm (~2.0 cm^{-1}, the green histograms) and (2) by simply shifting the MODIS SRF by −35.0 nm (~7.7 cm^{-1}, the red histograms). Although shifting MODIS band 27 SRF without correcting for the convolution error can produce a zero-biased match between MODIS and AIRS radiances, the std of the resulting error distribution (red histogram) is much wider than that which can be achieved using method 1 (green histogram in Figure 13). Most importantly, the −9.0 nm shift value is more consistent with a shift value derived from the MODIS-IASI intercalibration study shown in Figure 10, where we have to shift the MODIS band 27 SRF by −10.5 nm in order to match the observed MODIS and IASI radiances.

5. Large Spectral Gap Filling

The spectral region of MODIS band 29 spans from 1,114 to 1,231 cm^{-1}. There are only 34 channels out of the 2,211 FSR CrIS channels within MODIS band 29, covering less than 20% of the band region. AIRS has 70 channels within MODIS band 29 that cover less than 32% of the band region. The MODIS-AIRS or MODIS-CrIS intercalibration of band 29 requires the compensation for missing spectral information. The missing spectral information can be predicted using the available CrIS or AIRS spectral radiance with the regression relationship described in section 2. This section demonstrates the application of the spectral filling methodology for the calibration of MODIS band 29 using FSR CrIS and evaluates the filling accuracy and uncertainty. The application discussed here can be easily extended for the calibration of other broadband sensor channels that provide measurement in the overlapping spectral region (e.g., the ABI channel 11, AHI channel 11, SEVIRI channel 7, and VIIRS channel M14).

The MODIS band 29 is covered by IASI measurements, and the MODIS-IASI convolution error for band 29 is negligible as we have demonstrated via the simulation study in section 3. Therefore, the IASI data can be used as a solid reference to test the spectral gap filling methodology. The spectral gap filling errors can be characterized explicitly by directly comparing the IASI spectra within the band 29 region and the values predicted using the collocated CrIS spectra. The regression matrix A (see equations (7) and (8)) used for the spectral gap filling is trained using the sample IASI channel radiances that lie within the MODIS band 29 but not covered by CrIS and the corresponding CrIS spectra. Both IASI and CrIS spectra are generated by convolving the 14,600 monochromatic LBLRTM spectra (see section 2) with corresponding hyperspectral channel SRFs. In principle, the relationship between the radiances from 386 IASI channel and the radiances from 2,211 CrIS channels can then be explicitly established as

$$R_i^{gap} = \sum_{k=1}^{2211} a_{i,k} R_k^{CrIS}, \tag{9}$$

where i is the index of 386 IASI channels and k is the index of CrIS channels. The regression coefficient $a_{i,k}$, as the matrix element of regression matrix A can be given by the ordinary least squares solution

$$A = \mathscr{R}^{gap\,T} \mathscr{R}^{CrIS\,T} \left(\mathscr{R}^{CrIS} \mathscr{R}^{CrIS\,T} \right)^{-1}, \tag{10}$$

where $\mathscr{R}^{CrIS}$ is a 2,211×N_s matrix that represents the ensemble of CrIS spectra, and $\mathscr{R}^{gap}$ is a 386×N_s matrix that represents the ensemble of IASI gap spectra, N_s is the number of sample spectra used for the training. However, The matrix $\mathscr{R}^{CrIS\,T}\,\mathscr{R}^{CrIS}$ can be ill conditioned. Therefore, CrIS spectra are practically represented using their principal components (PCs)

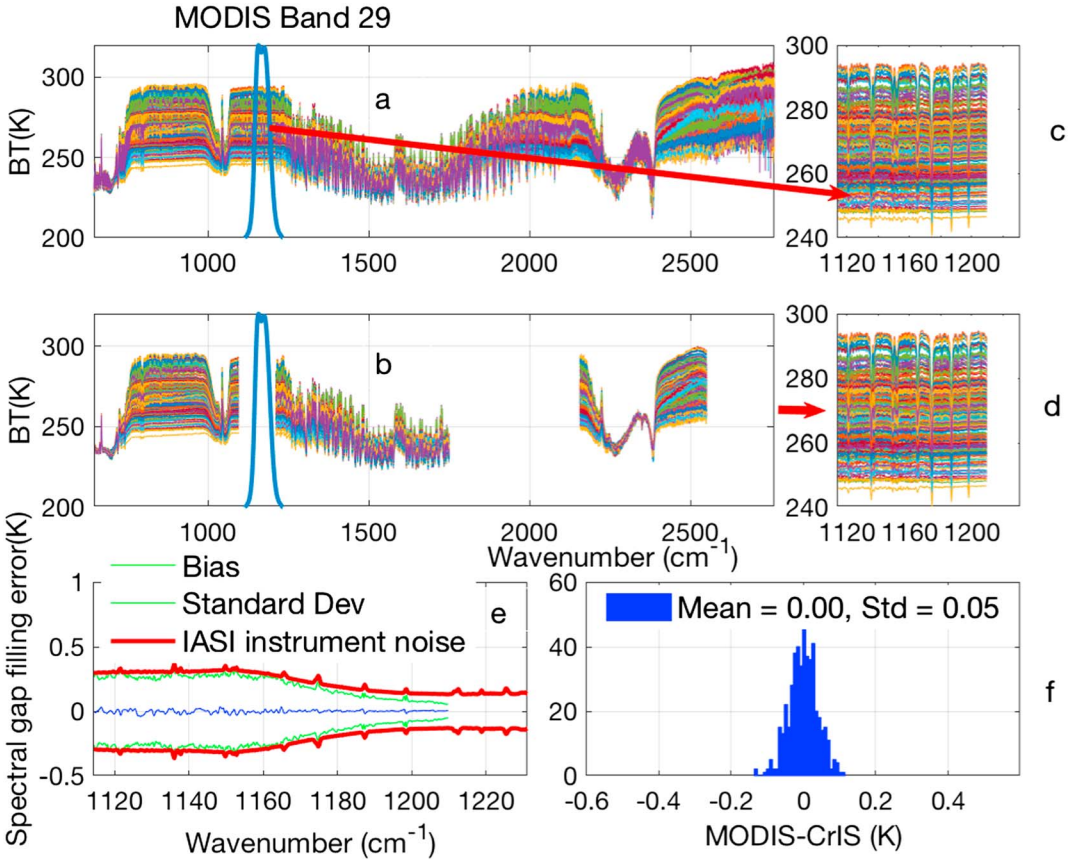

Figure 14. Using the CrIS spectra to predict the collocated IASI spectra within the spectral region covered by the MODIS band 29 but missed in CrIS measurement. (a) Selected IASI spectra on 17 September 2007; (b) the CrIS spectra generated using the IASI spectra; (c) the IASI spectra within the MODIS band 29; (d) the in-band IASI spectra predicted using the generated CrIS spectra; (e) the bias and the standard deviation values for the difference between the real in-band IASI spectra and the predicted values (the magnitude of the IASI instrument random noise are also plotted for reference); (f) the CrIS-MODIS (band 29) intercalibration errors due to the spectral gap filing errors. CrIS = Cross-track Infrared Sounder; IASI = Infrared Atmospheric Sounding Interferometer; MODIS = Moderate resolution Imaging Spectroradiometer.

$$\boldsymbol{R}^{\mathbf{CrIS}} = \boldsymbol{U}\boldsymbol{X}^{\mathbf{CrIS}} \tag{11}$$

where $\boldsymbol{U}$ is the PC matrix generated by applying a singular value decomposition on $\mathscr{R}^{\mathbf{CrIS}}$. $\boldsymbol{X}^{\mathbf{CrIS}}$ represents the PC scores of the CrIS spectra. If the number of PCs used to represent CrIS spectra is *npc*, the dimensions of $\boldsymbol{U}$ are 2,211×*npc*. The number of PCs used for the regression training can be adjusted based on the training and validation results. Using inadequate PC numbers may fail to accurately represent the CrIS spectra, while too many PCs can introduce instability in matrix inversion or cause overfitting. In our study, less than 50 PCs are used for the training. Therefore, the regression relationship between the IASI radiance in the gap region and the PC scores of the CrIS spectra can be derived as

$$A = \boldsymbol{R}^{\mathbf{gap}}\mathscr{X}^{\mathbf{CrIS}^T}\left(\mathscr{X}^{\mathbf{CrIS}}\mathscr{X}^{\mathbf{CrIS}^T}\right)^{-1}\mathbf{U}^T, \tag{12}$$

where $\mathscr{X}^{\mathbf{CrIS}}$ is the ensemble of PC scores and *A* is a matrix of 386×2,211. After *A* is derived, the spectral gap radiance for a given CrIS observation can be predicted as

$$\boldsymbol{R}^{\mathbf{gap}} = \boldsymbol{A}\cdot\boldsymbol{R}^{\mathbf{CrIS}}. \tag{13}$$

The regression coefficient matrix *A* trained for spectral gap filling is validated using independent data sets from real satellite observations. In order to provide a clean evaluation for the spectral gap filling errors that can be separated from other error sources, we convert IASI spectra to CrIS proxy spectra using a double

Fourier transform method to ensure a *perfect collocation*, instead of using real collocated CrIS measurements. The CrIS spectra are generated by a standard procedure that includes several steps: (1) Fourier transformation of IASI spectra to interferograms of 2.0 cm optical path difference; (2) deapodization of the IASI interferograms; (3) truncation of deapodized interferograms according to the FSR CrIS optical path difference of 0.8 cm; (4) applying the Blackman apodization to CrIS interferograms; and (5) inverse Fourier transformation of the interferograms to construct the CrIS spectra. A similar procedure has been used for postlaunch calibration assessment between IASI and CrIS, and the resampling error has been confirmed to be less than 0.02 K (L. Wang et al., 2012).

The IASI spectra used for validation are selected from observations on 1 September 2007. The subplot (a) of Figure 14 illustrates the distribution of the spectral radiances. The subplot (b) shows the FSR CrIS spectra generated from the IASI spectra. The subplot (d) plots the IASI spectral gap radiances predicted from the CrIS spectra. Those predicted spectra gap radiances well recovers the true spectral information that is demonstrated in the subplot (c). Subplot (e) of Figure 14 shows that the bias of the difference between the real in-band IASI spectra and the predicted ones is close to 0 in all spectral gap channels. The uncertainty of the prediction error is consistent with the IASI instrument noise level. The true IASI spectra are then convolved with the SRF of MODIS band 29 to obtain the collocated MODIS radiances. The convolution is also applied to the synthetic spectra that combines the CrIS spectra and the predicted IASI spectral gap radiances, and the results are compared with MODIS radiances obtained from the IASI spectra. The difference is shown as a histogram plot in subplot (f). The mean and standard value of the difference shown in subplot (f) confirms that the remaining systematic bias after the spectral gap filling is negligible and the uncertainty is about 0.05 K. The randomly distributed errors are mainly due to the instrument random noise in IASI data, and will not show up as intercalibration errors between space-time averaged observations.

6. Summary and Conclusion

We have studied the impact of convolution errors on the intercalibration between hyperspectral and broadband sensors. In order to fully benefit from the future calibration reference standard provide by CLARREO and to generate accurate long-term time series record for climate applications, large convolution errors need to be reduced to be smaller than or at least on the same order of magnitude of the CLARREO accuracy. Intercalibration convolution errors are fundamentally caused by the missing information due to spectral gaps, and the *coarseness* of the hyperspectral measurement characterized by the limited spectral resolution and the spectral overlapping between SRFs. IASI's high spectral resolution and continuous spectral coverage between 645 and 2,760 cm^{-1} makes the convolution error of MODIS-IASI intercalibration a negligible concern. The nominal spectral resolution of CrIS is coarser than IASI; therefore, the convolution errors between CrIS and MODIS are much bigger. Although the convolution errors for apodized CrIS measurements of bands 24, 25, 33, 34, 35, and 36 can still be viewed as significant as compared with the CLARREO calibration requirement, the corresponding errors for unapodized CrIS measurements are much smaller. The unapodized CrIS measurement causes much smaller errors in those bands because of its less spectral overlapping between adjacent SRFs. CrIS does not cover the complete spectral regions of the MODIS bands 21–22. The convolution errors introduced by both apodized and unapodized CrIS measurements for the intercalibration of those two MODIS bands are significant and similar in scale. AIRS provides a better spectral resolution than CrIS of the nominal resolution (but lower spectral resolution than the full-resolution CrIS for MWIR and SWIR bands) but can introduce larger convolution errors for the intercalibration of several MODIS bands due to the instrument spectral gaps or the missing information of bad channels.

We have also developed a correction algorithm that can reduce these errors. One of the significant advancements of our algorithm compared with previous studies is that we can accurately account for both the scene and the spectrally dependent convolution errors by taking advantage of the hyperspectral measurements. This is possible because of the spectral correlations in the measured hyperspectral data. Large scene-dependent, spectrally dependent convolution errors associated with MODIS-CrIS or MODIS-AIRS intercalibration can be well addressed by the regression-correction scheme using the coefficients obtained via the simulation study. The convolution errors after correction become negligible even according to the most stringent calibration standard that is required for the climate studies. The relationship between the convolution errors and the corresponding hyperspectral information derived from the radiative transfer simulation results

is further validated using the real MODIS-AIRS data. Our application study on real data demonstrates that intercalibration errors can be effectively reduced after correcting the MODIS-AIRS convolution errors. A better than 0.1 K consistency is demonstrated between the SNO observations of AIRS and IASI. The accurate characterization for the scene and spectrally dependent feature of the convolution errors also helps to reduce calibration uncertainties and therefore better evaluate other calibration errors. We demonstrate that the potential drifts in the SRFs of MODIS bands 25, 27, and 28 can be overestimated. For example, a shift of MODIS band 27 SRF by as much as −35 nm is needed in order to match the observed MODIS and AIRS observations. However, a shift of only −9.0 nm is needed after performing convolution error correction. This SRF shift value is more consistent with the shift obtained from the MODIS-IASI study. The spectral correlation relationship can also be used for the large spectral gap filling or spectral range extension. Our study using the real IASI data as the reference confirms that the spectral information that is missing but needed for the calibration of MODIS band 29 can be very accurately filled using the available CrIS measurements. The same spectral filling methodology can be applied for the intercalibration between MODIS band 29 and AIRS measurements. Methods developed in this paper can also be applied to intersatellite calibration in solar spectral regions.

Acknowledgments
This research was supported by the NASA CLARREO project and by the NOAA JPSS program. We thank AER Inc. for providing the LBRTM model used in this study. The NASA SMD High-End Computing (HEC) resources were used to support the LBLRTM radiative transfer calculations. The AIRS data (version 5) used for this study are from http://mirador.gsfc.nasa.gov, the MODIS data (version 3.0) are from https://ladsweb.nascom.nasa.gov/, and the IASI data are from https://www.bou.class.noaa.gov/.

References

AIRS Version 5 Documentation (2016). Retrieved from https://docserver.gesdisc.eosdis.nasa.gov/repository/Mission/AIS/3.3_ScienceDataProductDocumentation/3.3.4_ProductGenerationAlgorithms/V5_L1B_QA_QuickStart.pdf, (accessed on 13 Jan. 2016).

Aumann, H. H., Chahine, M. T., Gautier, C., Goldberg, M. D., Kalnay, E., McMillin, L. M., et al. (2003). AIRS/AMSU/HSB on the Aqua mission: Design, science objectives, data products, and processing systems. *IEEE Transactions on Geoscience and Remote Sensing*, *41*(2), 253–264. https://doi.org/10.1109/TGRS.2002.808356

Barnes, W. L., Pagano, T. S., & Salomonson, V. V. (1998). Prelaunch characteristics of the Moderate Resolution Imaging Spectroradiometer (MODIS) on EOS-AM1. *IEEE Transactions on Geoscience and Remote Sensing*, *36*(4), 1088–1100. https://doi.org/10.1109/36.700993

Cao, C., Goldberg, M., & Wang, L. (2009). Spectral bias characterization of historical HIRS using IASI observations for improved fundamental climate data records. *Journal of Atmospheric and Oceanic Technology*, *26*, 1378–1387. https://doi.org/10.1175/2009JTECHA1235.1

Chander, G., Hewison, T. J., Fox, N., Wu, X., Xiong, X., & Blackwell, W. J. (2013). Overview of intercalibration of satellite instruments. *IEEE Transactions on Geoscience and Remote Sensing*, *51*(3), 1056–1080. https://doi.org/10.1109/TGRS.2012.2228654

Chen, Y., & Han, Y. (2015). Evaluation of Different Calibration Approaches for S-NPP Cris Full Spectral Resolution SDR Processing. *2015 IEEE International Geoscience and Remote Sensing Symposium (IGARSS)* (pp. 2127–2130). https://doi.org/10.1109/IGARSS.2015.7326223

Clough, S. A., & Iacono, M. J. (1995). Line-by-line calculation of atmospheric fluxes and cooling rates II: Application to carbon dioxide, ozone, methane, nitrous oxide and the halocarbons. *Journal of Geophysical Research*, *97*(D14), 15,761–16,535. https://doi.org/10.1029/92JD01419

Efremova, B., Wu, A., & Xiong, X. (2014). Relative spectral response corrected calibration inter-comparison of S-NPP VIIRS and Aqua MODIS thermal emissive bands. *Proceedings of SPIE*, *9218*, 92180G. https://doi.org/10.1117/12.2061917

Goldberg, M., Ohring, G., Butler, J., Cao, C., Datla, R., Doelling, D., et al. (2011). The Global Space-based Inter-Calibration System (GSICS). *Bulletin of the American Meteorological Society*, *92*(4), 468–475.

Gunshor, M. M., Schmit, T. J., Menzel, W. P., & Tobin, D. C. (2009). Intercalibration of broadband geostationary imagers using AIRS. *Journal of Atmospheric and Oceanic Technology*, *26*(4), 746–758. https://doi.org/10.1175/2008JTECHA1155.1

Han, Y., Revercomb, H., Cromp, M., Gu, D., Johnson, D., Mooney, D., et al. (2013). Suomi NPP CrIS measurements, sensor data record algorithm, calibration and validation activities, and record data quality. *Journal of Geophysical Research: Atmospheres*, *118*, 12,734–12,748. https://doi.org/10.1002/2013JD020344

Hewison, T. J., Wu, X., Yu, F., Tahara, Y., & Koenig, M. (2013). GSICS inter-calibration of infrared channels of geostationary imagers using Metop/IASI. *IEEE Transactions on Geoscience and Remote Sensing*, *51*, 1056–1080.

Lee, F., Nelson, C. S., Dills, P., Riishojgaard, L. P., Jones, A., Li, L., et al. (2010). NPOESS: Next-generation operational global Earth observations. *Bulletin of the American Meteorological Society*, *91*(6), 727–740. https://doi.org/10.1175/2009BAMS2953.1

Li, Y., Wu, A., & Xiong, X. (2013). Evaluating calibration of MODIS thermal emissive bands using Infrared Atmospheric Sounding Interferometer measurements. *Proc. SPIE 8724, Ocean Sensing and Monitoring V*, 87240X (2013/06/03). https://doi.org/10.1117/12.2016621

Li, Y., Wu, A., & Xiong, X. (2016). Inter-comparison of S-NPP VIIRS and Aqua MODIS thermal emissive bands using hyper-spectral infrared sounder measurements as a transfer reference. *Remote Sensing*, *8*, 72.

Liu, X., Wu, W., Wielicki, B. A., Yang, Q., Kizer, S. H., Huang, X., et al. (2017). Spectrally dependent CLARREO infrared spectrometer calibration requirement for climate change detection. *Journal of Climate*, *30*(11), 3979–3998. https://doi.org/10.1175/JCLI-D-16-0704.1

Liu, X., Zhou, D. K., Larar, A. M., Smith, W. L., Schlüssel, P., Newman, S. M., et al. (2009). Retrieval of atmospheric profiles and cloud properties from IASI spectra using super-channels. *Atmospheric Chemistry and Physics*, *9*(23), 9121–9142. https://doi.org/10.5194/acp-9-9121-2009

Sohn, B. J., Kim, B.-R., & Lee, S.-S. (2010). Possible shift of spectral response function of the MODIS 6.8 μm water vapor channel causing a cold bias of 2–3 K. *Atmospheric Measurement Techniques*, *3*(6), 1667–1672. https://doi.org/10.5194/amt-3-1667-2010

Stamnes, K., Tsay, S.-C., Wiscombe, W., & Jayaweera, K. (1988). Numerically stable algorithm for discrete-ordinate-method radiative transfer in multiple scattering and emitting layered media. *Applied Optics*, *27*(12), 2502–2509. https://doi.org/10.1364/AO.27.002502

Sun, J., Xiong, X., Madhavan, S., & Wenny, B. N. (2014). Terra MODIS Band 27 electronic crosstalk effect and its removal. *IEEE Transactions on Geoscience and Remote Sensing*, *52*(3), 1551–1561. https://doi.org/10.1109/TGRS.2013.2252180

Tahara, Y., & Kato, K. (2008). New spectral compensation method for intercalibration with high spectral resolution sounder, *Japan Meteorological Agency Meteorological Satellite Center Tech. Note*, 52, 37 [Available online at http://mscweb.kishou.go.jp/monitoring/gsics/ir/techinfo.htm.]

Tobin, D. C., Revercomb, H. E., Moeller, C. C., & Pagano, T. S. (2006). Use of atmospheric infrared sounder high–spectral resolution spectra to assess the calibration of Moderate resolution Imaging Spectroradiometer on EOS Aqua. *Journal of Geophysical Research*, *111*, D09S05. https://doi.org/10.1029/2005JD006095

Wang, L., & Cao, C. (2008). On-orbit calibration assessment of AVHRR longwave channels on MetOp-A using IASI. *IEEE Transactions on Geoscience and Remote Sensing*, *46*(12), 4005–4013. https://doi.org/10.1109/TGRS.2008.2001062

Wang, L., Cao, C., & Ciren, P. (2007). Assessing NOAA-16 HIRS radiance accuracy using simultaneous nadir overpass observations from AIRS. *Journal of Atmospheric and Oceanic Technology*, *24*(9), 1546–1561. https://doi.org/10.1175/JTECH2073.1

Wang, L., Cao, C., & Goldberg, M. (2009). Intercalibration of GOES-11 and GOES-12 water vapor channels with MetOp IASI hyper-spectral measurements. *Journal of Atmospheric and Oceanic Technology*, *26*(9), 1843–1855. https://doi.org/10.1175/2009JTECHA1233.1

Wang, L., Han, Y., Weng, F., & Goldberg, M. (2012). Inter-comparison of NPP/CrIS radiances with VIIRS, AIRS, and IASI: A post-launch calibration assessment, Proc. SPIE 8528, Earth Observing Missions and Sensors: Development, Implementation, and Characterization II, 85280J (9 November 2012). https://doi.org/10.1117/12.978769

Wang, L., Wu, X., Goldberg, M., Cao, C., Li, Y., & Sohn, S. (2010). Comparison of AIRS and IASI radiances using GOES imagers as transfer radiometers toward climate data records. *Journal of Applied Meteorology and Climatology*, *49*(3), 478–492. https://doi.org/10.1175/2009JAMC2218.1

Wang, M., Naik, P., & Son, S.-H. (2016). Out-of-band effects of satellite ocean color sensors. *Applied Optics*, *55*(9), 2312–2323. https://doi.org/10.1364/AO.55.002312

Wielicki, B. A., Young, D. F., Mlynczak, M. G., Thome, K. J., Leroy, S., Corliss, J., et al. (2013). Achieving climate change absolute accuracy in orbit. *Bulletin of the American Meteorological Society*, *94*(10), 1519–1539. https://doi.org/10.1175/BAMS-D-12-00149.1

Wu, A., Xie, Y., Xiong, X., & Chu, I.-W. (2012). Assess calibration consistency of MODIS and AVHRR thermal infrared bands using SNO observations corrected for atmospheric effect. *Geoscience and Remote Sensing Letters*, *9*(3), 487–491. https://doi.org/10.1109/LGRS.2011.2172677

Wu, W., Liu, X., Zhou, D. K., Larar, A. M., Yang, Q., Kizer, S. H., & Liu, Q. (2017). The application of PCRTM physical retrieval methodology for IASI cloudy scene analysis. *IEEE Transactions on Geoscience and Remote Sensing*, *55*(9), 5042–5056. https://doi.org/10.1109/TGRS.2017.2702006

Wu, X., & Yu, F. (2013). Correction for GOES imager spectral response function using GSICS. Part I: Theory. *IEEE Transactions on Geoscience and Remote Sensing*, *51*(3), 1215–1223. https://doi.org/10.1109/TGRS.2012.2236100

Xiong, X., Wenny, B. N., Wu, A., & Barnes, W. L. (2009). MODIS onboard blackbody function and performance. *IEEE Transactions on Geoscience and Remote Sensing*, *47*(12), 4210–4222. https://doi.org/10.1109/TGRS.2009.2023317

Yu, F., & Wu, X. (2013). Correction for GOES imager spectral response function using GSICS. Part II: Applications. *IEEE Transactions on Geoscience and Remote Sensing*, *51*(3), 1200–1214. https://doi.org/10.1109/TGRS.2012.2236559